International Journal of Computational and Experimental Science and ENgineering (IJCESEN)

Vol. 10-No.4 (2024) pp. 1211-1222
http://www.ijcesen.com

ISSN: 2149-9144

Research Article

Investigation of heat generation calculations in numerical modelling of friction stir welding

Amal V. PURUSHOTHAMAN[1]*, S. MUTHUKUMARAN[2], Deepesh VIMALAN[3]

[1]Department of Metallurgical and Materials Engineering, National Institute of Technology Tiruchirappalli, Tiruchirappalli- 620015, Tamilnadu, India
* **Corresponding Author Email:** amalv123@gmail.com - **ORCID:** 0000-0003-4025-2010

[2]Department of Metallurgical and Materials Engineering, National Institute of Technology Tiruchirappalli, Tiruchirappalli- 620015, Tamilnadu, India
Email: smuthu@nitt.edu - **ORCID:** 0000-0002-1395-9240

[3]Quality, Bharat Heavy Electricals Limited, Tiruchirappalli -620014, Tamilnadu, India
Email: deepeshvimalan@gmail.com - **ORCID:** 0000-0003-2867-4229

Article Info:

DOI: 10.22399/ijcesen.558
Received : 24 October 2024
Accepted : 25 November 2024

Keywords :

Friction Stir Welding,
Numerical Modelling,
Heat Generation,
Material Science,
Finite Element Analysis.

Abstract:

Numerical modelling is a powerful tool for understanding the temperature distribution and material flow in Friction Stir Welding (FSW) and Friction Stir Processing (FSP). However, the lack of a suitable framework and difficulty in accurately estimating heat generation are crucial challenges in this area. This paper examined different approaches used by researchers to predict heat generation. Actual experimentation was conducted to ascertain the variation of normal force under different process parameters by varying the tool rotation rate and traverse speed. Investigation revealed that the magnitude of the normal force differs under various experimental conditions. However, most existing numerical models neglect this crucial variation of the normal force. The results necessitate adopting the CEL approach in future studies, as it effectively considers the variation in normal force, which can precisely predict heat generation.

1. Introduction

Friction stir welding (FSW) and friction stir processing (FSP) are some of the leading materials joining and processing technologies. FSW can produce high-quality welds without melting the materials, eliminating solidification defects. On the other hand, FSP improves the tribological and corrosion properties of the surface. Extensive research is being done on developing surface composites using FSP[1].

However, when a new material combination is to be welded or processed, a trial-and-error method has to be adopted to select proper processing parameters. This methodology is time-consuming and does not hold any analytical ground. If a robust numerical model is developed to simulate FSW/FSP, it can be effectively used to optimise the process parameters. Numerical models can estimate heat generation, temperature distribution, deformations, stress states, and material flow. Based on the predictions, a bottom-to-top approach can be used to design experiments to get suitable output characteristics without doing a large number of laboratory experiments.

The underlying mechanisms in FSW and FSP are highly complex. The heat generation mechanism is nonlinear and coupled to material plasticity. The nonlinearity is localised, and the exact boundary determination is also tricky [2]. In FSW and FSP, heat is generated by friction and plastic deformation. The heat generated by friction depends on normal force, material properties, actual contact area and relative sliding velocity between the surfaces. When FSW/ FSP begins, friction between the tool and workpiece generates heat. This heat raises the material temperature, changing properties such as thermal conductivity, convectivity, surface roughness, yield strength and flow stress. This leads to changes in the magnitude of the normal force exerted by the tool, the actual area of contact and relative velocity. As these parameters change, the heat generation rate counter changes. The heat generated by plastic deformation also depends on

equivalent stress and strain rate. This coupled and nonlinear variation of properties in a short period makes it very difficult to predict the heat generation in FSP and FSW.

There is uncertainty in selecting the proper framework for numerical models as there are both solid mechanics and fluid dynamics points of view [3]. Earlier researchers used Lagrangian, Eulerian, and Arbitrary Lagrangian-Eulerian (ALE) Frameworks to study the problems [4]. Nowadays, Computational Fluid Dynamics (CFD), Coupled Eulerian-Lagrangian (CEL) and Smoothed Particle Hydrodynamics (SPH) approaches are also used [5–7]. Researchers use different approaches for numerical studies and make different assumptions when defining heat generation.

Due to the complexities discussed above, the heat generation in friction stir welding is not considered accurate in most numerical models. This paper examines the different methods researchers adopt to calculate heat generation and explains the need to consider the variation of force in FSW numerical models.

2. Heat Generation Calculation in Literature

The earlier studies used experimental readings to calculate the heat generation for the numerical model. Fonda et al. [8] developed an inverse heat generation model to compute the heat generation from the experimental reading of the temperature. Then, three-dimensional temperature fields across the different zones were computed and used for further studies. A similar study was conducted by Khandkar et al. [9] by computing heat generation at each instant from the experimental torque reading. Hamilton et al. [10] used energy per unit length as the input parameter from the experimental readings. Torque was computed from the energy reading and was used for further calculations.

In later studies, heat generated by friction was computed as the product of frictional shear stress and relative velocity. Based on the approach, accuracy required, and computational cost, different researchers computed frictional shear stress by different means. The simplest of them is based on the Coulomb law of friction given in Equation 1.

$$\text{Frictional shear stress, } \tau = \mu p \quad (1)$$

Where μ is the coefficient of friction, and p is the normal pressure exerted by the tool on the workpiece. It is to be noted that there is no specific value for μ; different researchers are employing various sets of values. A few studies used constant values of μ [11–16], and a few others used temperature-dependent values [17–19].

A modified version of Coulomb's law is given by equation 2 and 3,

$$\tau = \mu p \quad if\ \mu p < \tau_{max} \quad (2)$$

$$\tau = \tau_{max}\ if\ \mu p > \tau_{max} \quad (3)$$

Here, the upper limit of frictional stress is limited by the yield shear strength of the material.

In the second approach, the magnitude of τ depends on slip and stick conditions. The state of slip and stick is determined by slip term δ which essentially depends on the material velocity. During pure slip, τ is calculated as the product of normal stress and coefficient of friction. On pure stick, τ is taken as shear yield strength, τ_y [20]. The value of τ in the partial stage of slip and stick is computed by equation 4. Most researchers use this equation for calculations [21–24].

$$\tau = (1-\delta)\mu p + \delta\tau_y \quad (4)$$

Some of the studies followed a similar approach where slip and stick cases are not considered separately; instead, τ is calculated based on the relative velocity, v_{rel} [2,25–27]. The term α_1 is a scaling constant. The τ is calculated with the equation 5.

$$\tau = -\mu p.\frac{\vec{v}_{rel}}{|\vec{v}_{rel}|}.\tanh(\alpha_1\|v_{rel}\|) \quad (5)$$

Norton's law is used in a few works to compute τ [28-43]. Material consistency factor α and relative velocity Δv are considered for the calculation. Material consistency factor is a term that resembles the normal pressure in calculation. The α value is adjusted in such a way that experimental and numerical model values match. Norton's law is commonly used when the CFD approach is used. The τ is calculated by equation 6.

$$\tau = \alpha(T)\ ||\Delta v||^{q-1}\ \Delta v \quad (6)$$

A few researchers define τ as the product of friction factor m and yield shear strength k [44,45,47,48]. They calculate the shear yield strength using the Von Mises yield criterion. A friction factor value is used either from old literature or by adjusting a random value to match the temperature in the experiment and numerical model. The τ is calculated by equation 7.

$$\tau = mk \quad (7)$$

The FSW process is an extensive deformation process. The classical Lagrangian approach has the

Table 1. *Analysis of literature.*

Year	Authors	Fictional shear stress calculation method	Normal Pressure / Force value	Approach	Remarks
2023	Jie Chen et al. [26]	$\tau = -\mu p.\frac{\vec{v}_{rel}}{\lvert\vec{v}_{rel}\rvert}.\tanh(\alpha_1\lVert v_{rel}\rVert)$	31 MPa	CFD	Based on experimental force readings.
2023	Lei Shi et al. [27]	$\tau = -\mu p.\frac{\vec{v}_{rel}}{\lvert\vec{v}_{rel}\rvert}.\tanh(\alpha_1\lVert v_{rel}\rVert)$	31 Mpa	CFD	Based on experimental force readings.
2022	Chengle Yang et al. [25]	$\tau = -\mu p.\frac{\vec{v}_{rel}}{\lvert\vec{v}_{rel}\rvert}.\tanh(\alpha_1\lVert v_{rel}\rVert)$	40.7 MPa	CFD	Calculates pressure from the experimental reading of force.
2022	Hepeng Jia et al. [30]	$\tau = (1-\delta)\mu p + \delta\tau_y$	60 MPa	CFD	The pressure value is from the experimental reading.
2022	Pardeep Pankaj et al. [31]	$\tau = (1-\delta)\mu p + \delta\tau_y$	Not specified	CFD	Uses experimental force reading to calculate frictional stress
2022	Hua Ji et al. [32]	$\tau = (1-\delta)\mu p + \delta\tau_y$	Not specified	CFD	Uses experimental force reading to calculate frictional stress
2022	Pardeep Pankaj et al.[33]	$\tau = (1-\delta)\mu p + \delta\tau_y$	Not specified	CFD	Uses experimental force reading to calculate frictional stress
2021	D.G.Andrade et al. [29]	$\tau = \alpha(T)\,\lvert\lvert\Delta v\rvert\rvert^{q-1}\,\Delta v$	90 MPa	ALE	Material consistency factor is used. A trial-and-error method is used to find the value of α. The same data is used for different speeds.
2021	Renju Mohan et al. [34]	$\tau = (1-\delta)\mu p + \delta\tau_y$	200 N	CFD	The same force data from the literature is used for nine simulations.
2020	Vasanthakumar Pandian et al. [14]	$\tau = \mu p$	5kN	-	Force value from an experiment is used.
2020	Yanning Guo et al. [16]	$\tau = \mu p$	10 kN	-	Force value is taken from other literature.
2020	P Prakash et al. [22]	$\tau = (1-\delta)\mu p + \delta\tau_y$	12 MPa	CFD	Pressure value from old literature is used for four simulations.
2020	H A Derazkola et al.[23]	$\tau = (1-\delta)\mu p + \delta\tau_y$	Not specified	CFD	Value from old literature is used for 12 combinations in simulation.
2020	Ming Zhai et al. [24]	$\tau = (1-\delta)\mu p + \delta\tau_y$	4.2 kN, 6.1 kN	CFD	Experimental readings from 2 cases are used for simulation.
2019	Nirav P.Patel et al. [21]	$\tau = (1-\delta)\mu p + \delta\tau_y$	~ 6 kN	Not Specified	Force value from old literature
2019	G Chen et al. [35]	$\tau = 12.5 + m\frac{\sigma_y}{\sqrt{3}}$	12.5 MPa	CFD	Constant pressure is used for shoulder action. The Norton model is used for shear stress calculation from the pin side.
2018	G Chen et al. [19]	$\tau = \mu p$	50 MPa	CFD	Pressure value from old literature is used for five different speeds.
2018	G Chen et al. [12]	$\tau = \mu p$	50 MPa	CFD	Pressure value from old literature is used.

2018	Z Sun et al. [36]	$\tau = (1-\delta)\mu p + \delta\tau_y$	30 MPa	CFD	Experimental force data is used for frictional stress calculation.
2023	Omar S. Salih et al. [37]	$\tau = \mu p$	Computed	CEL	Pressure between the surfaces is calculated in a numerical model.
2022	AK Choudhary et al. [11]	$\tau = \mu p$ $\tau = \tau_{max}, if\ \mu p > \tau_{max}$	Computed	CEL	Pressure is calculated using the penalty contact algorithm.
2022	Peihao Geng et al. [13]	$\tau = \mu p$ $\tau = \tau_{max}, if\ \mu p > \tau_{max}$	Computed.	CEL	The penalty contact method is used to calculate the normal pressure between the tool and the workpiece.
2022	Murat Turkan et al. [18]	$\tau = \mu p$ $\tau = \tau_{max}, if\ \mu p > \tau_{max}$	Computed	CEL	The compressive force is calculated.
2021	B Meyghani [2]	$\tau = -p\frac{v_g}{\lvert v_g\rvert}.g(v_g)$	Calculating pressure with a modified fem model.	CSM	FEM software calculates the relative velocity at each increment. Then, the modified friction model calculates the corresponding pressure and shear stress.
2020	H.J. Zhang et al. [15]	$\tau = \mu p$	computed	CEL	The CEL approach calculates the interfacial stress between the tool and the workpiece.
2019	Salloomi [17]	$\tau = \mu p$ $\tau = \tau_{max}, if\ \mu p > \tau_{max}$	Computed	ALE	ALE approach is adopted to predict the Normal force.
2019	Ansari Mohammad Ali et al. [38]	$\tau = \mu p$ $\tau = \tau_{max}, if\ \mu p > \tau_{max}$	Computed	CEL	The model predicts axial force.
2023	Z. Zhang et al. [39]	NA	NA	Not Specified	Heat source magnitude is adjusted based on experimental temperature reading.
2022	J.Y. Sheikh-Ahmad et al. [40]	NA	NA	Not Specified	Heat source magnitude is adjusted based on experimental temperature reading.
2021	El-Moayed et al. [41]	not defined	26.5 MPa	Not Specified	Calculated heat flux from the same value of force for all 16 simulations.
2021	Gaoqiang Chen et al. [42]	NA	NA	FVM	Heat flux is calculated based on the temperature reading from the experiment.
2019	M I Costa et al. [43]	NA	NA	CSM	Heat flux is calculated based on experimental torque reading.
2023	Jiaqing You et al. [44]	$\tau = m\tau_{max}$	NA	CSM	Shear yield strength is considered.
2020	Bo Du et al. [45]	$\tau = m\tau_{max}$	NA	CSM	Shear yield strength is considered.
2020	Md Perwej Iqbal et al. [46]	$\tau = m\tau_{max}$	NA	CSM	Shear yield strength is considered.
2020	Wenshen Tang et al. [47]	$\tau = m\tau_{max}$	NA	CSM	Shear yield strength is considered.

disadvantage of withstanding limited deformation. The pure Eulerian approach can withstand large deformation, but modelling corresponding tool-workpiece interactions is challenging. So, most of the researchers chose the CFD approach over the CSM approach. The CFD approach is suitable for handling material flow and velocity calculations. The disadvantage of the CFD approach lies in the difficulty of computing the normal force at the interface [5,6].

Significant research works in numerical simulation of FSP and FSW in the past five years are examined in Table 1 to understand how existing numerical studies calculate τ and normal force.

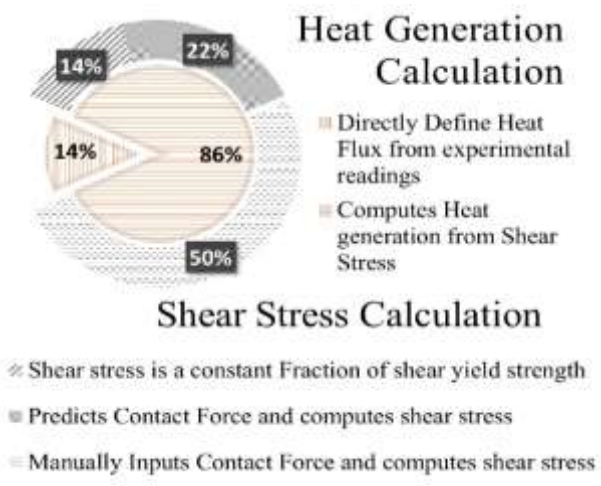

Figure 1. *Percentage of studies using different types of heat generation calculations.*

Except for the 14% of the models which directly define the surface heat flux as boundary conditions based on the experimental readings [39–43], the rest of the models compute heat generation from τ (Figure 1). In that, a few models estimate τ based on shear yield strength [44–48], and the rest of the works consider normal force in the calculation. Many researchers use the predefined value of normal force for a material combination from old literature [12,16,19,21–23]. The material might be the same, but the process parameters used in the new and old studies differ. Some researchers use force readings from experiments to calculate heat generation in numerical simulation [14,24–27,30–33,36,41]. On tabulating, it is understood that only 22% of the works examined in this study have tried predicting the normal force for heat generation calculation. In 50% of the works the force value must be fed manually.

Researchers also reported that thermal contact conductance varies with the normal force [10], which also affects the temperature distribution. Normal force is one of the main factors affecting heat generation, so it should be accurately considered while simulating FSW and FSP.

In this work, actual FSW is done to analyse how normal force varies with different process parameters. A numerical simulation is done using a CEL approach to see how it predicts the normal force during welding.

3. Experimental Procedure

Heat generation calculation is similar for FSP and FSW in numerical simulations. Bead-on-plate FSW was used in this study to simplify the experimentation. FSW has two phases, viz the plunge phase and the traverse phase. In the plunge phase, the rotating tool starts rubbing the surface and plunges to a predefined depth. A plunge depth of 5 mm was used for all the experiments in this study. The initial tool plunging rate was 10 mm/min. The table traverses for 80mm horizontally in the traverse phase, keeping the plunge depth constant.

One of the aims of this study was to check whether the normal force remains the same for different processing conditions during FSW. Tool rotational rate and traverse speed were varied to generate nine different experimental conditions, as given in Table 2. FSW was done on all these nine experimental conditions, and the normal force was measured from the Friction Stir Welding Machine. The impact of the normal force was examined by monitoring the instantaneous temperature recorded at the tool-workpiece interface. For experimentation, AA6061 plate was used. The tool was made of EN32 steel. The shoulder diameter of the tool was 16 mm, and the pin diameter was 5 mm. The depth of the pin was 4.5mm. The Plate dimensions were 100 mm x 150 mm x 6mm. A 4-axis friction stir machine was used for experimentation (Figure 2). The machine can record the movement of the tool, workpiece and the instantaneous value of normal force. The instantaneous surface temperature was recorded using an Infrared camera (Figure 3).

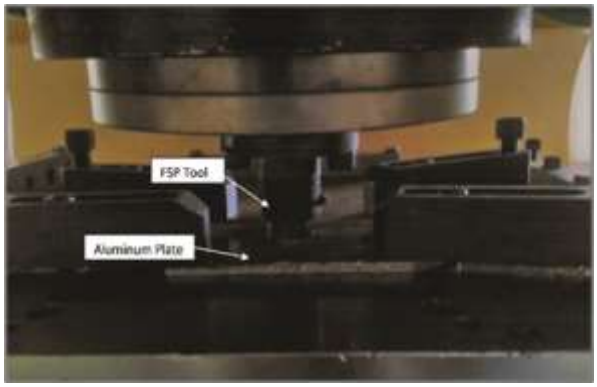

Figure 2. *Sample in FSW machine.*

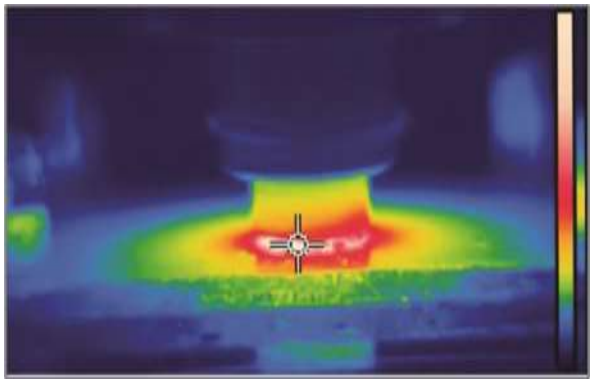

Figure 3. *Temperature measurement using IR camera during.*

Table 2. *Process parameters.*

Experiment Number	Tool Rotation Rate (RPM)	Traverse Speed (mm/min)
1	600	30
2	600	60
3	600	120
4	1200	30
5	1200	60
6	1200	120
7	2000	30
8	2000	60
9	2000	120

4. Numerical Simulation

A CEL analysis is used to numerically model friction stir processing. In a CEL framework, the plate is modelled in an Eulerian framework so that it can handle large deformations. The tool is modelled as a rigid body in a Lagrangian framework. The equations will be first solved in the Eulerian framework to analyse the interactions between the Lagrangian tool and the Eulerian workpiece. Then, the deformation gradient and Jacobian determinant are solved using the Lagrangian framework. Hence, this approach can calculate the interfacial stress. The calculated normal force will vary based on the plastic state of the plate. So, this approach is more realistic to the actual condition, whereas most of the studies use a constant value of normal force. A Johnson-Cook material model is used to predict the material behaviour at different temperatures, strains and strain rates [11]. The tool with a shoulder diameter of 16 mm and a pin diameter of 5 mm is used. The depth of the pin is 4 mm. A total of 6328 C3D10MT tet elements were used to build the geometry of the tool. The approximate global size of the edge is 1.5 mm. The plate is modelled using Eulerian EC3D8RT hex elements. The actual plate size is 100 mm x 150 mm x 5 mm. In order to capture the flash formation, the Eulerian domain defined

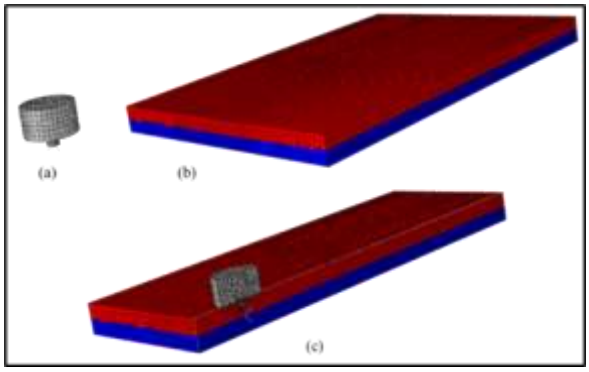

Figure 4. *Discretisation of geometry (a) meshed view of tool; (b) meshed view of Eulerian domain; (c) cross section of assembled view.*

has an additional height of 5 mm above the surface of the plate (Figure 4). Even though the Eulerian domain has more volume than the plate dimension, the material is initially assigned only to the volume corresponding to the plate dimensions. Later, the material can flow within this domain based on the interactions. A central area of the part where the tool and plate interact is made with fine elements having an approximate size of 1.25 mm. The size of the elements gradually increases to 2.5 mm towards the periphery. A total of 52,560 elements were used to define the Eulerian volume, which was 100 mm x 150 mm x 15 mm.

A penalty contact condition is assigned for the contact interaction between the tool surfaces and the plate. A Coulomb's friction law is considered for heat generation. Heat generation due to friction is given by equation 7.

$$Q_f = \mu PV \tag{7}$$

where μ is the coefficient of friction taken as 0.25. P is the instantaneous value of normal pressure calculated by the study. V is the instantaneous value of relative velocity between the tool and workpiece. Heat generation due to plastic deformation is also considered in calculations as per equation 8.

$$Q_p = \eta \sigma_e \, \dot{\varepsilon}_e \tag{8}$$

Where η is the plastic deformation heat conversion efficiency assumed to be 0.9. σ_e is the equivalent stress, and $\dot{\varepsilon}_e$ is the equivalent strain rate,

Net heat generation is the sum of frictional heat generation and plastic work heat generation.

$$Q = Q_f + Q_p \tag{9}$$

The momentum and energy balance equations used in this study are the same as those used in Chen et al. 's study [12].

The initial temperature for all the parts was set to 300 ℃. The plate was fixed with the encastre boundary condition. The tool was given a rotational degree of freedom about the Z axis and translational degrees of freedom in the z and y directions. One simulation was performed with the same combination of process parameters as that used in experiment 5.

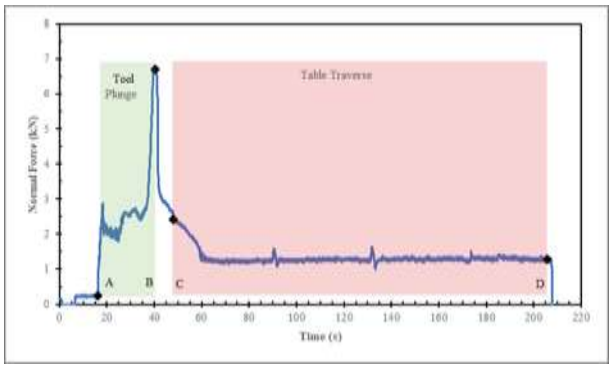

Figure 5. *Variation of normal force during traverse.*

5. Results

5.1 Normal Force Variations

The general pattern of normal force response in FSW is explained by the reading from experiment 7 in Figure 5. The normal force acting on the tool rises as the rotating tool plunges into the workpiece during the plunge phase (A-B). The increase in force is steeper near the end of the plunge when the shoulder starts to touch the surface. A dwell period exists between the tool plunge and table traverse phases (B-C). During this time, normal force reduces. As the table moves, normal force remains almost constant during the traverse period (C-D). The average normal force is the mean of the force response in the traverse phase. Similarly, the average interface temperature is the mean of temperatures recorded in the traverse phase.

Table 3 *Force and Temperature readings.*

Exp No	Tool Rotation Rate (RPM)	Traverse Speed (mm/min)	Average Normal Force (kN)	Average Interface Temperature (℃)
1	600	30	3.02	406
2	600	60	3.39	371
3	600	120	4.34	348
4	1200	30	1.66	442
5	1200	60	2.32	440
6	1200	120	2.67	417
7	2000	30	1.25	469
8	2000	60	1.71	468
9	2000	120	2.16	460

The average normal force and average interface temperature from all nine experiments are tabulated in **Table 3**. Comparing the nine experiment results, it is evident that the average normal force differs with process parameters.

5.2 Average Normal Force and Tool Rotation Rate

For experiments 1,4 and 7, the tool rotation rates are 600 RPM, 1200 RPM and 2000 RPM, respectively. The traverse speed is 30 mm/min for all three experiments. The instantaneous variation of normal forces with time is shown in Figure 7. The force magnitudes in the plunge and traverse phases are highest for the sample processed with 600 RPM; the corresponding average normal force was 3.02 kN. When the tool rotation rate was changed to 2000 RPM, the average normal force dropped to 1.25 kN. A similar pattern is observed among experiments 2,5,8 and 3,6,9, which are represented in Figure 8 and **Hata! Başvuru kaynağı bulunamadı.**Figure 9, respectively. Consolidated data shown in Figure 6 indicates that the average normal force is less when the experiment is done with a high tool rotation rate.

5.3 Average Normal Force and Traverse Speed

Normal force responses for experiments 7,8, and 9, having table traverse speeds of 30 mm/min, 60

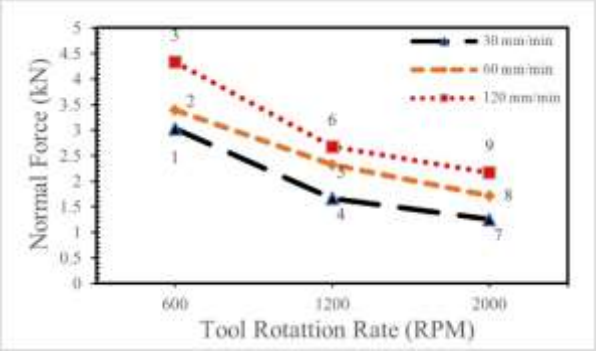

Figure 6. *Variation of average normal force with tool rotation rate.*

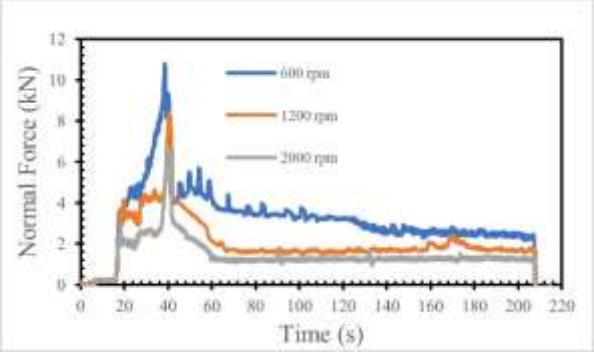

Figure 7. *Instantaneous normal force at 30 mm/min for 3 tool rotational rates.*

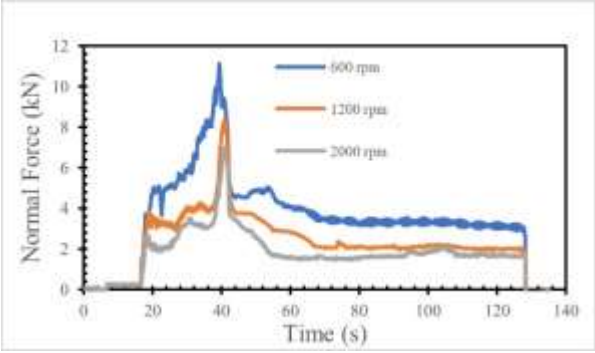

Figure 8. *Instantaneous normal force at 60 mm/min for 3 tool rotational rates.*

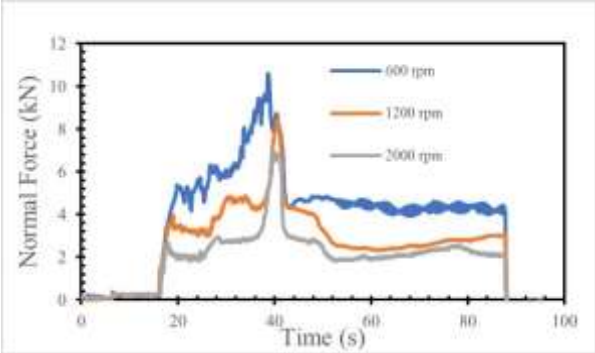

Figure 9. *Instantaneous normal force at 120 mm/min for 3 tool rotational rates.*

mm/min and 120 mm/min, respectively, are plotted in Figure 10. The tool rotation rate is 2000 RPM for these three experiments. The variation of the normal force in the plunge phase was the same for all three experiments. However, force varied in different patterns by the start of the traverse phase. The average force was the least for the experiment with a traverse speed of 30 mm/min. The average normal force was higher when processing was done with higher traverse speeds. The same pattern was observed in experiments 1,2,3 and 4,5,6. Consolidated data is shown in Figure 11.

6. Discussion

From results 0, it is clear that average normal force values are lower when the tool rotation rate is high.

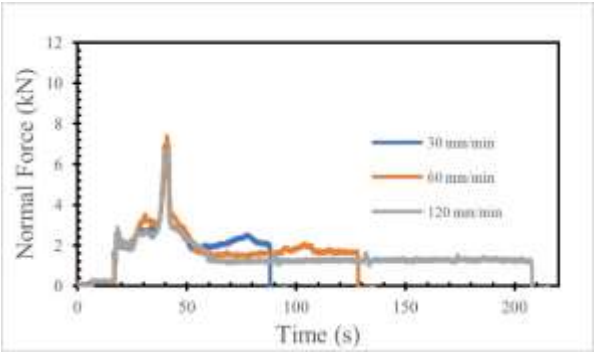

Figure 10. *Instantaneous normal force at 2000 rpm for 3 traverse speeds.*

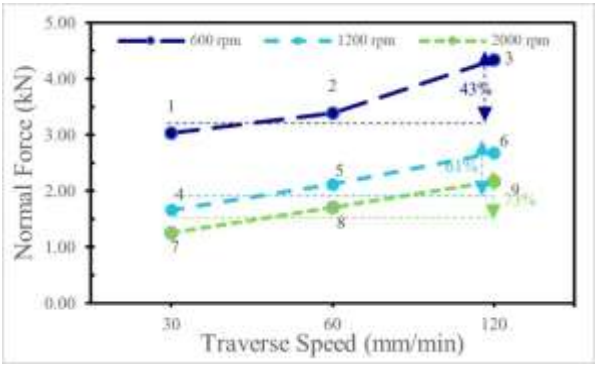

Figure 11. *Variation of average normal force with traverse speed.*

Rotation of the tool at higher rates generates more heat at the interface. The material will be softer at higher temperatures, so the magnitude of force needed to stir the material will be less. For different traverse speeds, the average interface temperatures ranged from 460 ℃ to 469 ℃ when the tool rotation rate was 2000 RPM. The corresponding average normal force ranged from 2.16 kN to 1.25 kN. Furthermore, for experiments with 600 RPM, average interface temperatures ranged from 348 ℃ to 406 ℃, and the corresponding average normal force ranged from 4.34 kN to 3.02 kN (Figure 12).

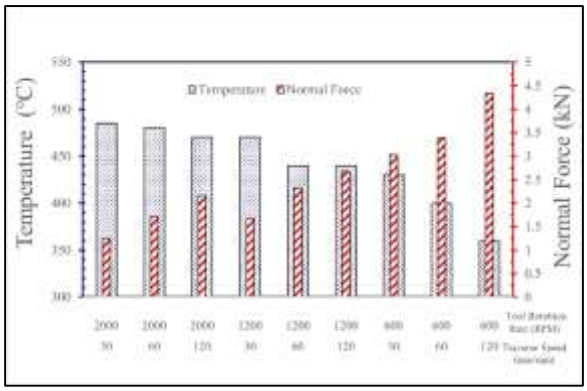

Figure 12. *Average normal force and average temperatures for all experiments.*

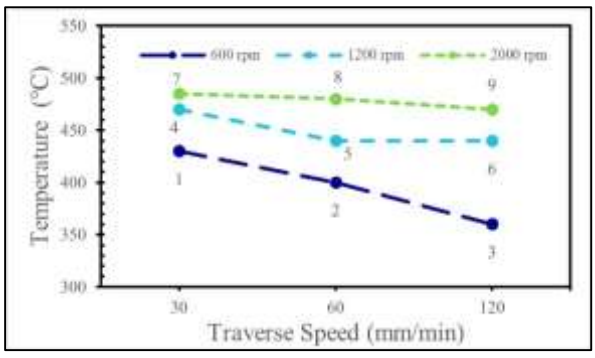

Figure 13. *Variation of average interface temperature with traverse speed.*

Among all the experiments, the highest temperature developed is 469 ℃ for 2000 RPM and 30 mm/min traverse speed. The tool's slow traverse helps to accumulate more heat at the interface. The average normal force acting in this case is 1.25 kN. On the other hand, the average normal force value is 4.33 kN when the tool rotation rate is 600 RPM, and the traverse rate is 120 mm/min. As heat transfer time is less at higher traverse speeds, the temperature developed is 348 ℃ only. Also, a greater volume of material must be moved per time at higher traverse speeds, so more force is required to stir the region. Consolidated data shown in Figure 13 implies that the average normal force value and average interface temperature values are inversely proportional.

The CEL model predicts the instantaneous value of normal force experienced by the tool. The pattern of force predicted is very similar to the actual case. The normal force rises to a peak value in the plunge phase and drops to a lower value afterwards, as represented in Figure 14. The temperature of one point just below the surface is also plotted. The temperature also rises to a peak value of 800K in the plunge phase; thereafter, it gradually decreases. The results show that the CEL approach can predict force variations. In this study, the force predictions are much higher than those of the actual experimentation. The main reason for this is the adoption of mass scaling to reduce computational time. As mentioned in previous sections, ambiguity in choosing the friction coefficient value and friction law can also lead to inaccuracies.

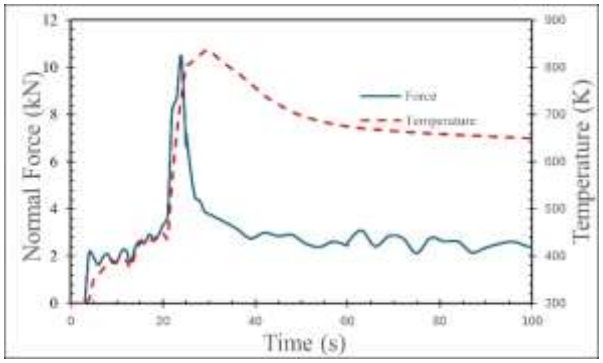

Figure 14. *Temperature and Force variation predictions.*

Results 0 clearly show that the average normal force differs for different process parameters. This implies that if the magnitude of the normal force is not correct in the numerical model, there will be a significant error in the heat generation calculation. However, from the literature review, it is understood that most researchers are feeding the same normal force value irrespective of the process parameters for the numerical model. To correct this error approaches like CEL should be used to predict the variation of the normal force.

The normal force is a response indicating the plate material's plastic state. The more plastic the material, the lesser the force needed and the harder the material, the higher the force needed to stir the material. So, the force response can be considered as a bulk property of the system. On the other hand, most researchers validate their model with medium to far-range temperature fields that are very insensitive to interfacial frictional behaviour. The temperature value in numerical simulations can be easily altered by adjusting the associated parameters [6], and researchers fail to cross-check whether other output fields are similar to the actual experimentation. So, when validating FSW models, researchers should give more importance to the force response than temperature to ensure the model's accuracy.

7. Conclusions

Overall, this study analysed how existing numerical simulations calculate heat generation. It is understood that most of the studies give the least importance to the value of normal force. Actual experiments were performed to find the variation pattern of the normal force in FSW. An interesting trend observed was that the temperature raised in the material was inversely proportional to the normal force acting on the tool.

The experiments show that the normal force's magnitude is not the same for different process parameter combinations. However, the same value of normal force is used in most numerical simulations. Feeding a constant value of normal force will lead to inaccurate heat generation rate calculation in numerical simulation. Most present studies validate their model by comparing experimental results of interface temperature with simulation results alone. However, a robust model should be able to predict the normal force and validate multiple parameters to ensure accuracy. In that case, the CEL approach will be most suitable for the numerical simulation of Friction Stir Welding and Processing. Even though the existing models can predict different output fields and can be used for further studies like phase changes and residual stress calculation, the inaccuracy in the heat generation calculation limits the potential of numerical simulation. Heat generation is as reported elsewhere [49,50] is studied in the literature.

Author Statements:

- **Ethical approval:** The conducted research is not related to either human or animal use.

- **Conflict of interest:** The authors declare that they have no known competing financial interests or personal relationships that could have appeared to influence the work reported in this paper
- **Acknowledgement:** The authors declare that they have nobody or no-company to acknowledge.
- **Author contributions:** The authors declare that they have equal right on this paper.
- **Funding information:** The authors declare that there is no funding to be acknowledged.
- **Data availability statement:** The data that support the findings of this study are available on request from the corresponding author. The data are not publicly available due to privacy or ethical restrictions.

References

[1]El-Sayed, M.M., Shash, A.Y., Abd-Rabou, M., and ElSherbiny, M.G. (2021) Welding and processing of metallic materials by using friction stir technique: A review. *Journal of Advanced Joining Processes*. 3.

[2]Meyghani, B. (2021) A modified friction model and its application in finite-element analysis of friction stir welding process. *Journal of Manufacturing Processes*. 72;29–47. https://doi.org/10.1016/j.jmapro.2021.10.008

[3]Dialami, N., Chiumenti, • M, Cervera, • M, and Agelet De Saracibar, C (2017) Challenges in Thermo-mechanical Analysis of Friction Stir Welding Processes. *Archives of Computational Methods in Engineering*. 24;189–228. DOI 10.1007/s11831-015-9163-y

[4]Chiumenti, M., Cervera, M., Agelet de Saracibar, C., and Dialami, N. (2013) Numerical modeling of friction stir welding processes. *Computer Methods in Applied Mechanics and Engineering*. 254;353–369. https://doi.org/10.1016/j.cma.2012.09.013

[5]Meyghani, B. and Wu, C. (2020) Progress in Thermomechanical Analysis of Friction Stir Welding. *J. Mech. Eng*. 33;12. https://doi.org/10.1186/s10033-020-0434-7

[6]Wang, X., Gao, Y., Liu, X., McDonnell, M., and Feng, Z. (2021) Tool-workpiece stick-slip conditions and their effects on torque and heat generation rate in the friction stir welding. *Acta Materialia*. 213;116969. https://doi.org/10.1016/j.actamat.2021.116969

[7]Meyghani, B., Awang, M.B., and Teimouri, R. (2021) Prediction of the Temperature Behaviour During Friction Stir Welding (FSW) Using Hyperworks®. in: *Lecture Notes in Mechanical Engineering, Springer, Singapore*, pp. 119–130.

[8]Fonda, R.W. and Lambrakos, S.G. (2002) Analysis of friction stir welds using an inverse problem approach. *Science and Technology of Welding and Joining*. 7 (3); 177–181. DOI:10.1179/136217102225002682

[9]Khandkar, M.Z.H., Khan, J., and Reynolds, A.P. (2003) Prediction of temperature distribution and thermal history during friction stir welding: Input torque based model Multiphysics Multiscale Modeling: Sweating-boosted Hybrid Cooling with Water Dripping for Thermal Power Plant Application View project. *Science and Technology of Welding and Joining*. 8 (3);165–174. http://dx.doi.org/10.1179/136217103225010943

[10]Hamilton, C., Dymek, S., and Sommers, A. (2008) A thermal model of friction stir welding in aluminum alloys. *International Journal of Machine Tools & Manufacture*. 48;1120–1130. https://doi.org/10.1016/j.ijmachtools.2008.02.001

[11]Choudhary, A.K. and Jain, R. (2022). Numerical prediction of various defects and their formation mechanism during friction stir welding using coupled Eulerian-Lagrangian technique. *Mechanics of Advanced Materials and Structures* 30(12); 2371-2384. https://Doi.Org/10.1080/15376494.2022.2053911.

[12]Chen, G., Li, H., Wang, G., Guo, Z., Zhang, S., Dai, Q., et al. (2018) Effects of pin thread on the in-process material flow behavior during friction stir welding: A computational fluid dynamics study. *International Journal of Machine Tools and Manufacture*. 124;12–21. https://doi.org/10.1016/j.ijmachtools.2017.09.002

[13]Geng, P., Morimura, M., Wu, S., Liu, Y., Ma, Y., Ma, N., et al. (2022) Prediction of residual stresses within dissimilar Al/steel friction stir lap welds using an Eulerian-based modeling approach. *Journal of Manufacturing Processes*. 79;340–355. https://doi.org/10.1016/j.jmapro.2022.05.001

[14]Pandian, V. and Kannan, S. (2020) Numerical prediction and experimental investigation of aerospace-grade dissimilar aluminium alloy by friction stir welding. *Journal of Manufacturing Processes*. 54;99–108. https://doi.org/10.1016/j.jmapro.2020.03.001

[15]Zhang, H.J., Sun, S.L., Liu, H.J., Zhu, Z., and Wang, Y.L. (2020) Characteristic and mechanism of nugget performance evolution with rotation speed for high-rotation-speed friction stir welded 6061 aluminum alloy. *Journal of Manufacturing Processes*. 60;544–552. https://doi.org/10.1016/j.jmapro.2020.10.081

[16]Guo, Y., Ma, Y., Zhang, X., Qian, X., and Li, J. (2020) Study on residual stress distribution of 2024-T3 and 7075-T6 aluminum dissimilar friction stir welded joints. *Engineering Failure Analysis*. 118; 104911.https://doi.org/10.1016/j.engfailanal.2020.104911

[17]Salloomi, K.N. (2019) Fully coupled thermomechanical simulation of friction stir welding of aluminum 6061-T6 alloy T-joint. *Journal of Manufacturing Processes*. 45;746–754. https://doi.org/10.1016/j.jmapro.2019.06.030

[18]Türkan, M. and Karakaş, Ö. (2022) Numerical modeling of defect formation in friction stir welding. *Materials Today Communications*. 31;103539. https://doi.org/10.1016/j.mtcomm.2022.103539

[19]Chen, G., Ma, Q., Zhang, S., Wu, J., Zhang, G., and Shi, Q. (2018) Computational fluid dynamics simulation of friction stir welding: A comparative study on different frictional boundary conditions.

Journal of Materials Science and Technology. 34 (1), 128–134. https://doi.org/10.1016/j.jmst.2017.10.015

[20]Schmidt, H., Hattel, J., and Wert, J. (2004) An analytical model for the heat generation in friction stir welding. *Modelling and Simulation in Materials Science and Engineering*. 12 (1), 143–157. DOI: 10.1088/0965-0393/12/1/013

[21]Patel, N.P., Parlikar, P., Singh Dhari, R., Mehta, K., and Pandya, M. (2019) Numerical modelling on cooling assisted friction stir welding of dissimilar Al-Cu joint. *Journal of Manufacturing Processes*. 47;98–109. https://doi.org/10.1016/j.jmapro.2019.09.020

[22]Prakash, P., Anand, R.S., and Jha, S.K. (2020) Prediction of weld zone shape with effect of tool pin profile in friction stir welding process. *Journal of Mechanical Science and Technology*. 34 (1), 279–287. https://doi.org/10.1007/s12206-019-1229-6

[23]Derazkola, H.A., Eyvazian, A., and Simchi, A. (2020) Modeling and experimental validation of material flow during FSW of polycarbonate. *Materials Today Communications*. 22;100796. https://doi.org/10.1016/j.mtcomm.2019.100796

[24]Zhai, M., Wu, C.S., and Su, H. (2020) Influence of tool tilt angle on heat transfer and material flow in friction stir welding. *Journal of Manufacturing Processes*. 59;98–112. https://doi.org/10.1016/j.jmapro.2020.09.038

[25]Yang, C., Dai, Q., Shi, Q., Wu, C., Zhang, H., and Chen, G. (2022) Flow-coupled thermo-mechanical analysis of frictional behaviors at the tool-workpiece interface during friction stir welding. *Journal of Manufacturing Processes*. 79;394–404. https://doi.org/10.1016/j.jmapro.2022.05.003

[26]Chen, J., Wang, X., Shi, L., Wu, C., Liu, H., and Chen, G. (2023) Numerical simulation of weld formation in friction stir welding based on non-uniform tool-workpiece interaction: An effect of tool pin size. *Journal of Manufacturing Processes*. 86;85–97. https://doi.org/10.1016/j.jmapro.2022.12.052

[27]Shi, L., Chen, J., Yang, C., Chen, G., and Wu, C. (2023) Thermal-fluid-structure coupling analysis of void defect in friction stir welding. *International Journal of Mechanical Sciences*. 241;107969. https://doi.org/10.1016/j.ijmecsci.2022.107969

[28]Dialami, N., Chiumenti, M., Cervera, M., Segatori, A., and Osikowicz, W. (2017) Enhanced friction model for Friction Stir Welding (FSW) analysis: Simulation and experimental validation. *International Journal of Mechanical Sciences*. 133;555–567. https://doi.org/10.1016/j.ijmecsci.2017.09.022

[29]Andrade, D.G., Leitão, C., Dialami, N., Chiumenti, M., and Rodrigues, D.M. (2021) Analysis of contact conditions and its influence on strain rate and temperature in friction stir welding. *International Journal of Mechanical Sciences*. 191;106095. https://doi.org/10.1016/j.ijmecsci.2020.106095

[30]Jia, H., Wu, K., and Sun, Y. (2022) Numerical and experimental study on the thermal process, material flow and welding defects during high-speed friction stir welding. *Materials Today Communications*. 31; 103526.https://doi.org/10.1016/j.mtcomm.2022.103526

[31]Pankaj, P., Tiwari, A., Dhara, L.N., and Biswas, P. (2022) Multiphase CFD simulation and experimental investigation of friction stir welded high strength shipbuilding steel and aluminum alloy. *CIRP Journal of Manufacturing Science and Technology*. 39;37–69. https://doi.org/10.1016/j.cirpj.2022.07.001

[32]Ji, H., Deng, Y.L., Xu, H.Y., Yin, X., Zhang, T., Wang, W.Q., et al. (2022) Numerical modeling for the mechanism of shoulder and pin features affecting thermal and material flow behavior in friction stir welding. *Journal of Materials Research and Technology*. 21;662–678.

[33]Pankaj, P., Tiwari, A., Medhi, T., and Biswas, P. (2022) Multi-species transport CFD simulation and experimental verification for material flow properties in dissimilar friction stir welding. *Materials Today Communications*. 33;104959. https://doi.org/10.1016/j.mtcomm.2022.104959

[34]Mohan, R., Jayadeep, U.B., and Manu, R. (2021) CFD modelling of ultra-high rotational speed micro friction stir welding. *Journal of Manufacturing Processes*. 64;1377–1386. https://doi.org/10.1016/j.jmapro.2021.02.060

[35]Chen, G., Wang, G., Shi, Q., Zhao, Y., Hao, Y., and Zhang, S. (2019) Three-dimensional thermal-mechanical analysis of retractable pin tool friction stir welding process. *Journal of Manufacturing Processes*. 41;1–9. https://doi.org/10.1016/j.jmapro.2019.03.022

[36]Sun, Z., Wu, C.S., and Kumar, S. (2018) Determination of heat generation by correlating the interfacial friction stress with temperature in friction stir welding. *Journal of Manufacturing Processes*. 31; 801–811. https://doi.org/10.1016/j.jmapro.2018.01.010

[37]Salih, O.S., Ou, H., and Sun, W. (2023) Heat generation, plastic deformation and residual stresses in friction stir welding of aluminium alloy. *International Journal of Mechanical Sciences*. 238;107827. https://doi.org/10.1016/j.ijmecsci.2022.107827

[38]Ansari, M.A., Samanta, A., Behnagh, R.A., and Ding, H. (2019) An efficient coupled Eulerian-Lagrangian finite element model for friction stir processing. *International Journal of Advanced Manufacturing Technology*. 101(5–8); 1495–1508. https://doi.org/10.1007/s00170-018-3000-z

[39]Zhang, Z., Tan, Z.J., Wang, Y.F., Ren, D.X., and Li, J.Y. (2023) The relationship between microstructures and mechanical properties in friction stir lap welding of titanium alloy. *Materials Chemistry and Physics*. 296;127251. https://doi.org/10.1016/j.matchemphys.2022.127251

[40]Sheikh-Ahmad, J.Y., Deveci, S., Almaskari, F., and Rehman, R.U. (2022) Effect of process temperatures on material flow and weld quality in the friction stir welding of high density polyethylene. *Journal of Materials Research and Technology*. 18;1692–1703. DOI:10.1016/j.jmrt.2022.03.082

[41]El-Moayed, M.H., Shash, A.Y., Rabou, M.A., and El-Sherbiny, M.G.D. (2021) A coupled statistical and numerical analysis of the residual properties of AA6063 friction stir welds. *Journal of Advanced*

Joining Processes. 3;1-17. DOI: 10.1016/j.jajp.2021.100042

[42]Chen, G., Zhu, J., Zhao, Y., Hao, Y., Yang, C., and Shi, Q. (2021) Digital twin modeling for temperature field during friction stir welding. *Journal of Manufacturing Processes*. 64;898–906. https://doi.org/10.1016/j.jmapro.2021.01.042

[43]Costa, M.I., Leitão, C., and Rodrigues, D.M. (2019) Parametric study of friction stir welding induced distortion in thin aluminium alloy plates: A coupled numerical and experimental analysis. *Thin-Walled Structures*. 134;268–276. https://doi.org/10.1016/j.tws.2018.10.027

[44]You, J., Zhao, Y., Miao, S., Lin, Z., Yu, F., Dong, C., et al. (2023) Effects of welding physical fields on the microstructure evolution during dynamic-stationary shoulder friction stir welding. *Journal of Materials Research and Technology*. 23;3219–3231. https://doi.org/10.1016/j.jmrt.2023.01.228

[45]Du, B., Yang, X., Tang, W., and Sun, Z. (2020) Numerical analyses of material flows and thermal processes during friction plug welding for AA2219 aluminum alloy. *Journal of Materials Processing Technology*. 278;116466. https://doi.org/10.1016/j.jmatprotec.2019.116466

[46]Iqbal, M.P., Tripathi, A., Jain, R., Mahto, R.P., Pal, S.K., and Mandal, P. (2020) Numerical modelling of microstructure in friction stir welding of aluminium alloys. *International Journal of Mechanical Sciences*. 185;105882. https://doi.org/10.1016/j.ijmecsci.2020.105882

[47]Tang, W., Yang, X., Li, S., Du, B., and Li, H. (2020) Numerical and experimental investigation on friction stir welding of Ti- and Nb-modified 12 % Cr ferritic stainless steel. *Journal of Manufacturing Processes*. 59;223–237. https://doi.org/10.1016/j.jmapro.2020.09.059

[48]Iqbal, M.P., Jain, R., and Pal, S.K. (2019) Numerical and experimental study on friction stir welding of aluminum alloy pipe. *Journal of Materials Processing Technology*. 274;116258. DOI:10.1016/J.JMATPROTEC.2019.116258

[49]S, M. K., V A, N., & A, R. (2024). Modal and harmonic analysis of femur bone using different boundary conditions by Finite Element Analysis. *International Journal of Computational and Experimental Science and Engineering*, 10(4);621-629. https://doi.org/10.22399/ijcesen.364

[50]Kabashi, G., Kola, L., Kabashi, S., & Ajredini, F. (2024). Assessment of climate change mitigation potential of the Kosovo energy and transport sector. *International Journal of Computational and Experimental Science and Engineering*, 10(3);517-526. https://doi.org/10.22399/ijcesen.325